Journal of Catalysis **189,** 314–325 (2000)
doi:10.1006/jcat.1999.2704, available online at http://www.idealibrary.com on IDEAL®

Methane Dehydro-aromatization under Nonoxidative Conditions over Mo/HZSM-5 Catalysts: EPR Study of the Mo Species on/in the HZSM-5 Zeolite

Ding Ma, Yuying Shu, Xinhe Bao, and Yide Xu[1]

State Key Laboratory of Catalysis, Dalian Institute of Chemical Physics, Chinese Academy of Sciences, 457 Zhongshan Road, P.O. Box 110, Dalian 116023, People's Republic of China

Received April 23, 1999; revised August 26, 1999; accepted October 4, 1999

EPR characterization of the Mo species on/in the HZSM-5 zeolite is described. Four different EPR signals, denoted as signals A, B, D, and E, respectively, have been recorded on the Mo/HZSM-5 sample during its stepwise reduction by methane. Different Mo species were identified on the basis of their reducibility and the nature of the signal concerned. There are two kinds of Mo species on the Mo/HZSM-5 sample, which are located at different positions on/in the HZSM-5 zeolite. The first kind of the Mo species is polynuclear and located on the external surface. They are either in the octahedral-coordinated MoO_3 crystallite form (denoted as MoO_3oct) or in the MoO_x form with a square-pyramidal coordination (denoted as MoO_xsqu). The second kind of the Mo species is associated with the Al atom in the lattice channels of the zeolite. The Mo species associated with Al are mononuclear species, which migrate or diffuse into the channels of the HZSM-5 during calcination. The EPR signals of migrating Mo ion (signals D and E) have hyperfine structures which are caused by the interaction between the Mo species and the lattice Al atom. And the corresponding Mo species are located at two different positions close to the Bronsted Al atoms: Al(I) $\cdots$ MoO_x and Al(II) $\cdots$ MoO_x. The order of reducibility of these four kinds of species is as follows: MoO_3oct $\approx$ MoO_xsqu $>$ Al(I) $\cdots$ MoO_x $>$ Al(II) $\cdots$ MoO_x. It was found that the O_2^- species might exist on the surface of the Mo/HZSM-5 catalyst during the induction period of the reaction. The variation of the different Mo species in a 6%Mo/HZSM-5 sample during the reaction course is illustrated, and the relationship between the catalytic performance and the intensity of the ESR spectra is discussed. It is proposed that Mo_2C is located at the external surface, while partial reduced Mo species associated with the Al atom is inside the channel during the reaction. Both of these Mo species play a key role in methane dehydro-aromatization.

Key Words: **methane dehydro-aromatization; Mo/HZSM-5; EPR; Mo species.**

INTRODUCTION

Recently, great attention has been focused on zeolite-supported catalysts (1–6), as their framework can play the role of stabilizing the loaded transition-metal ions (TMI), especially when the TMI migrate into the intracrystalline cavities and/or channels of the zeolites. On the other hand, by combining acid sites with TMI, one can build up a series of bifunctional catalysts with unique catalytic properties. As a typical example, it was reported in 1993 that methane could be directly transformed into benzene and toluene over the Mo/HZSM-5 catalyst in a flow reactor mode in the absence of O_2 (7). It has been proposed that the channel structure and acidity of zeolites as well as the valence states and location of Mo species on/in the HZSM-5 are crucial factors for a good catalytic performance of the catalyst. Great efforts have been made to improve the catalytic performances (8–14), to elucidate the nature of the Mo precursors which may relate to the formation of active Mo species, and to explore the possible mechanism of the reaction (9, 15–22). By characterization of the catalyst with FT-IR, ISS, NH_3-TPD (15, 16, 18), NH_4OH extraction (19), and ^{27}Al and ^{29}Si MAS-NMR techniques (23), it was revealed that various Mo species existed on/in the zeolite in different ways. NH_4OH extraction (19) and ^{27}Al and ^{29}Si MAS-NMR techniques (23) suggested that there may exist four kinds of Mo species on/in the HZSM-5 zeolite because of different preparation conditions. These four kinds of species are the tetrahedral-coordinated species, the octahedral-coordinated species, the MoO_3 crystallite, and the $Al_2(MoO_4)_3$ crystallite. TPR and UV Raman spectra have showed the existence of the MoO_3 crystallite and the octahedral-coordinated polymolybdate species (24).

To pursue this point further, we described here detailed EPR characterization of the changes of the Mo species in the Mo/HZSM-5 samples after calcination at 773 K and reduction by CH_4 at different temperatures as well as the changes of Mo species in Mo/HZSM-5 catalysts during methane dehydro-aromatization. We also attempted to correlate the changes of Mo species during the reaction with the activity of the catalyst.

[1] To whom correspondence should be addressed. Fax: 0086-411-4694447. E-mail: xuyd@ms.dicp.ac.cn.

0021-9517/00 $35.00

EXPERIMENTAL

1. Preparation of Mo/HZSM-5 Samples

HZSM-5 with Si/Al = 25, supplied by Nan Kai university, was used without further treatment. HZSM-5 powder of 10 g was impregnated with 10 ml of aqueous solution, containing the desirable amount of ammonium heptamolybdate (AHM), then dried at room temperature for 12 h. After the samples were further dried at 373 K for 8 h and calcined in air at 773 K for 5 h, they were crushed and sieved to 20- to 60-mesh granules for catalytic evaluations. Hereafter, the Mo/HZSM-5 catalysts with different Mo loadings were denoted as *x*Mo/HZSM-5, where *x* is the nominal Mo content in weight percent.

2. Catalytic Evaluation

All the reactions were carried out with a 6.2-mm i.d. quartz tubular fixed-bed reactor. Usually, the reactor was charged with 0.2 g of catalyst. To preheat the feed, 2 g of quartz chips was put on top of the catalyst layer. All gases used in this work were UHP grade without further purification. For running the reaction, the catalyst was first heated under a He stream (15 ml/min) to 973 K in 1 h and maintained at 973 K for 30 min under atmospheric pressure. A gas mixture of 9.5% N_2/CH_4 was admitted into the reactor, which was adjusted through a Brooks mass flow controller at a space velocity of 1500 ml of N_2/CH_4 per gram of catalyst per hour. N_2 (9.5%) in the CH_4 reactant was used as an internal standard as reported by Lunsford *et al.* (15) to enable us to measure the CH_4 conversion, selectivity of all products, and the carbonaceous deposits on-line. Hydrocarbon products including C_1–C_3 alkanes, alkenes and C_6–C_{10} aromatics were analyzed by an on-line gas chromatograph (Shimadzu GC-9A) equipped with a flame ionization detector (FID) using an OV-101 6201 column and a thermal conductive detector (TCD) using a HayeSep-D column. All reaction rates were expressed in nmol of CH_4/(g cat s). For simplicity, hereafter, r_{CH_4} denotes the methane depletion rate; r_{CO} denotes the CO formation rate; r_{HC} denotes the C_2–C_4 hydrocarbon formation rate; r_{AR} denotes the aromatics (benzene, toluene, naphthalene, etc.) formation rate; and r_C denotes the formation rate of carbonaceous deposits. All the formation rates of the products are expressed on the basis of consumed methane.

3. EPR Studies

In all cases EPR studies were performed on a JEOL ES-EO3X X-band spectrometer at room temperature. A microwave frequency ν of 9.42 GHz with a power of 1 mW was used. The relative spin concentration and g factor were calculated by taking the signal of manganese as an internal standard. The spectra have been digitized and integrated twice by a NEXTSTEP workstation to calculate the relative spin concentration.

A specially designed ESR cell, which can be used at the same time as a fixed-bed flow reactor, was employed. The set-up consists of a gas flow section, a reactor section, and an evacuation section as shown in Fig. 1. Usually, it was charged with 0.15 g (20–60 mesh) of sample. A gas either as the pretreater or as the reactant was introduced through a glass capillary tube (1-mm i.d.), with the tip inserted into the bottom of the catalyst bed. The gas flowed upward through

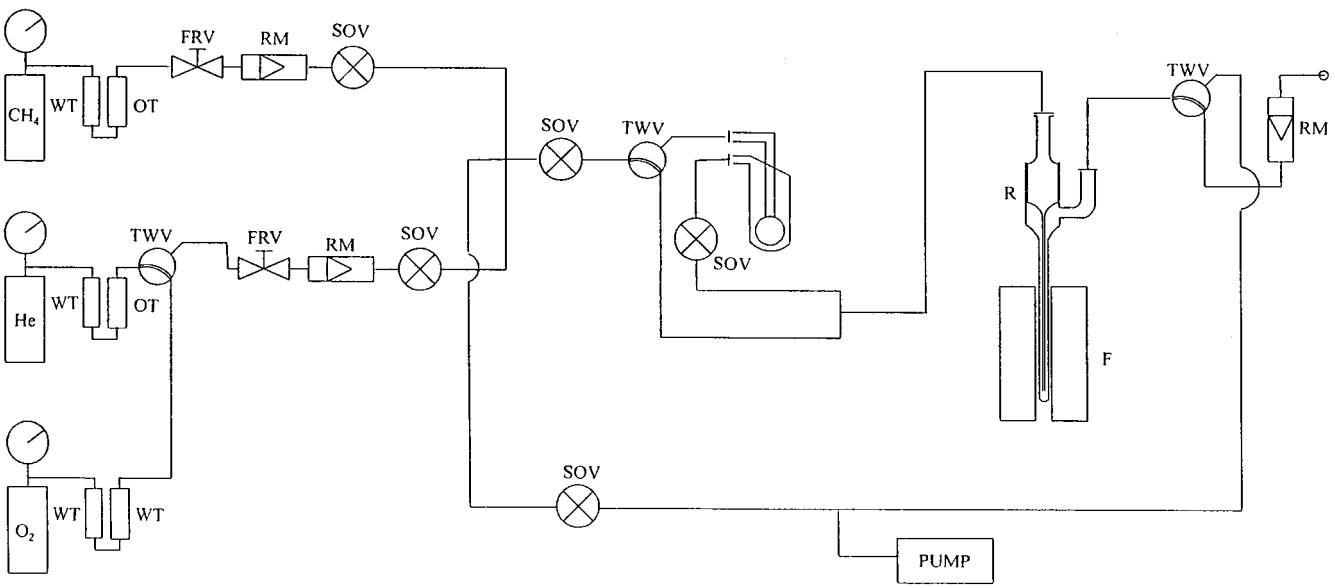

FIG. 1. The sketch of the experimental set-up. WT, water trap; OT, oxygen trap; FRV, flowing-regulating valve; RM, rotameter; SOV, shut-off valve; TWV, three-way valve; R, reactor; F, furnace.

the catalyst bed and then flowed out via a three-way valve (Whitey SS-42 × S6MM). When the system switched from one gas to another, the residual gas in the system was evacuated by a mechanic pump via the three-way valve. The sample was heated in a custom-made furnace and usually the temperature was programmed and controlled by a XMT-type temperature controller. After the reaction or the pretreatment, the reactor was transferred into the resonance cavity of the EPR spectrometer without contacting air. Therefore, it is possible to detect and measure the EPR signals of the sample under the conditions similar to the methane dehydro-aromatization reaction.

EPR measurements were performed in two different ways. In the first case the Mo/HZSM-5 sample was reduced with CH_4 (1500 ml/(g cat h)) at 373, 573, and 773 K for 1 h, respectively. It was then reduced at 973 K for 0.5 and 1 h (0.5 + 0.5 h) successfully to characterize the reducibility of the Mo species located on different positions on/in the zeolite. In the other case, the sample was pretreated with the same procedure as in methane dehydro-aromatization reaction on the Mo/HZSM-5 catalysts at 973 K. The EPR signals were recorded for treating the catalysts with He at 973 K for 0.5 h and running the reaction for 0.5, 1(0.5 + 0.5), and 3 h (0.5 + 0.5 + 2 h) at 973 K, respectively. After the reaction was quenched to room temperature, the EPR spectra were recorded.

UHV-grade methane and helium were used. Both gases passed through an oxygen trap and a water trap for further purification before they were introduced into the reactor.

RESULTS

1. *EPR Characterization of the Reduction of Mo Species by CH_4*

Figure 2 shows the EPR spectra of 2Mo/HZSM-5 catalyst after stepwise reduction with flowing CH_4 at different temperatures. When the catalyst was treated and reduced in a CH_4 stream (1500 ml/(g cat h)) at 373 K for 1 h, two EPR signals, located at $g = 2.003$ and $g_\perp = 1.943$, and $g_\parallel = 1.882$, respectively, could be obviously detected (Fig. 2b). The isotropic signal of $g = 2.003$ is from the free electron of carbonaceous deposits formed from the residual template due to its incomplete decomposition during the synthesis (4). If the HZSM-5 sample was treated under the same conditions, no other signals except for the signal at $g = 2.003$ could be detected. Furthermore, when the 2Mo/HZSM-5 sample was calcined in an oxygen flow at 813 K for 1 h and subsequently treated with flowing CH_4 at 373 K or a higher temperature for 1 h, no isotropic signal at $g = 2.003$, but only the high field signal, could be recorded. On the other hand, the high field signal, denoted as A, with $g_\perp = 1.943$ and $g_\parallel = 1.882$ can be ascribed to the Mo^{5+} species on the catalyst surface similar to that found in Refs (4, 25–29).

With an increase in the reduction temperature to 573 K for 1 h, the color of the sample turned from blue white to light gray, and a new signal, denoted as B, appeared with the same $g_\parallel$ value, but a larger anisotropic $g_\perp$ value of 1.954 (Fig. 2c). This signal overlapped with the high field signal A, giving a broader signal (see Fig. 2c). No obvious changes can be monitored for the signal at $g = 2.003$. With a further increase in the reduction temperature to 773 K, a more complicated and broader signal denoted as C (it refers to the overall Mo^{5+} signal and is not marked in Fig. 2) appeared. In fact, the signal C consists of many slight splitted lines (Fig. 2d). At the same time the color of the sample turned to gray. The splitting in $g_\perp$ is clearer than that in $g_\parallel$, as shown in Fig. 2d. These splitted signals on the Mo/HZSM-5 samples were unique and have not been reported before. A similar splitting structure has been observed by Kucherov *et al.* on Cr/HZSM-5 and V/HZSM-5 catalysts (30, 31). They found a Cr^{5+} signal with about 15 component peaks on Cr/HZSM-5 (30) and ascribed it to the hyperfine structures induced by the lattice Al^{3+} ions ($I = 5/2$). Accordingly, they suggested that three discrete positions of Cr^{5+} with different distortions must exist in ZSM-5. Since the existence of a site with two nearby Al^{3+} ions is of lesser possibility in the ZSM-5 zeolite, which has a Si/Al atomic ratio of 25, we suggest that there are two different kinds of sites on the zeolite surface which have particular interaction with Mo species. This, in the end, will lead to the appearance of the two sets of splitted signals. More careful analysis revealed that the signal C might consist of overlapped signals. In fact, it is composed of the signals A and B and two new six-line axial symmetric signals, denoted as D and E, respectively. The signal D has $g_\perp = 1.953 (A_\perp = 7.6 \pm 0.1)$ and $g_\parallel = 1.895$, and the signal E has $g_\perp = 1.982 (A_\perp = 9 \pm 0.1)$ and $g_\parallel = 1.920$. Both the signals D and E have hyperfine structures. The hyperfine structures are superimposed on each other as illustrated in Fig. 2d. With the reduction temperature further increased to 973 K, i.e., the temperature for methane dehydro-aromatization, and maintained at this temperature for 0.5 h, the color of the sample turned to black with a remarkable increase in the intensity of the signal at $g = 2.003$ (Fig. 2e). The shape and the line width of this signal are in good agreement with the coke formed at high temperatures. For example, Lange *et al.* ascribed the signal to condensed aromatic or graphite-like coke (32). The remarkable increase in the intensity of the signal with $g = 2.003$ is due to the coke formation, as compared with the signal in Fig. 2d. At the same time, the intensity of so-called signal C decreases significantly, particularly the high field part of it. However, both signals of D and E still can be clearly observed. If the reduction/reaction lasted for 0.5 h more at 973 K, the intensity of the signal C decreased and the intensity of the signal at $g = 2.003$ increased (see Fig. 2f).

Usually, for Mo-containing catalysts, the EPR signals detected correspond to only a small fraction of the overall Mo present (3). By double integrating the as-recorded spectra

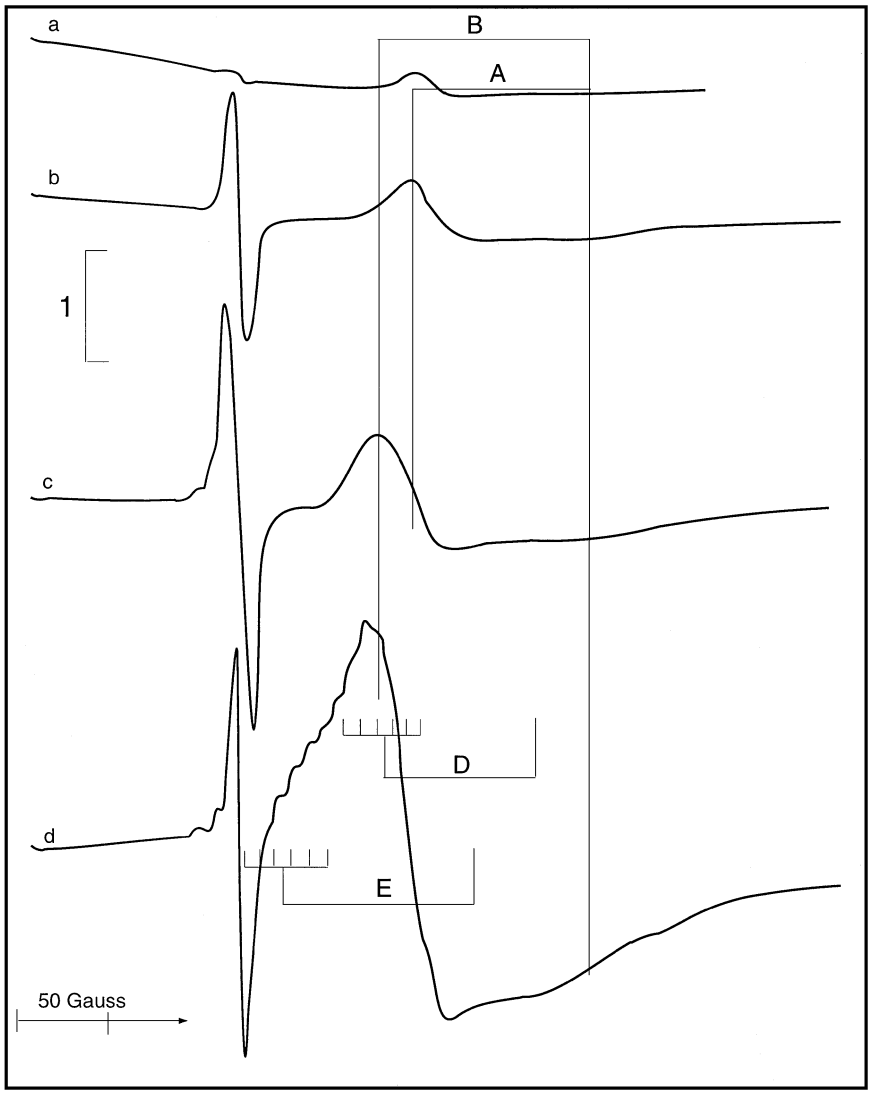

FIG. 2. ESR spectra of 2%Mo/HZSM-5 reduced at (a) RT for 1 h, (b) 373 K for 1 h, (c) 573 K for 1 h, (d) 773 K for 1 h, (e) 973 K for 0.5 h and (f) 973 K for 1 h.

and comparing them with those of the reference, one can estimate the EPR-detectable Mo amount. For example, the maximum intensity of the 2Mo/HZSM-5 catalyst converted to spin concentration corresponds to about 15% of the total molybdenum content in the sample.

The corresponding spectra for both 6Mo/HZSM-5 and 10Mo/HZSM-5 samples recorded at different reduction temperatures are shown in Figs. 3 and 4, respectively. The four Mo^{5+} signals, i.e., signals A, B, D, and E, as have been mentioned above, could be detected. The higher the Mo loading, the higher the intensity of the overall Mo^{5+} signal, particularly, in the temperature range of 573–973 K. The quantitative results are shown in Fig. 5, obtained by double integrating the overall Mo signal after the reduction at 773 K. The EPR signals that correspond to Mo^{5+} species are still observable, even if the sample was reduced by CH_4 at 973 K for 1 h.

Another important feature of the high Mo loading sample is that its hyperfine structure is not so obvious as that of the 2Mo/HZSM-5. Therefore, the hyperfine structure is related to the dispersion of the Mo species. For the 10Mo/HZSM-5 sample reduced with CH_4 at 573 K for 1 h, the signal recorded mainly consists of signal B and the two poorly resolved splitting signals, D and E. Possibly the signals of D and E are so weak that they are fully immersed within the signal B. On the other hand, the EPR spectra recorded from catalysts of different Mo loadings after their reduction at high temperature do not change very much.

2. EPR Spectra of 6Mo/HZSM-5 Recorded under Reaction Conditions

The EPR spectra of the 6Mo/HZSM-5 recorded after different pretreatments and different reaction times were

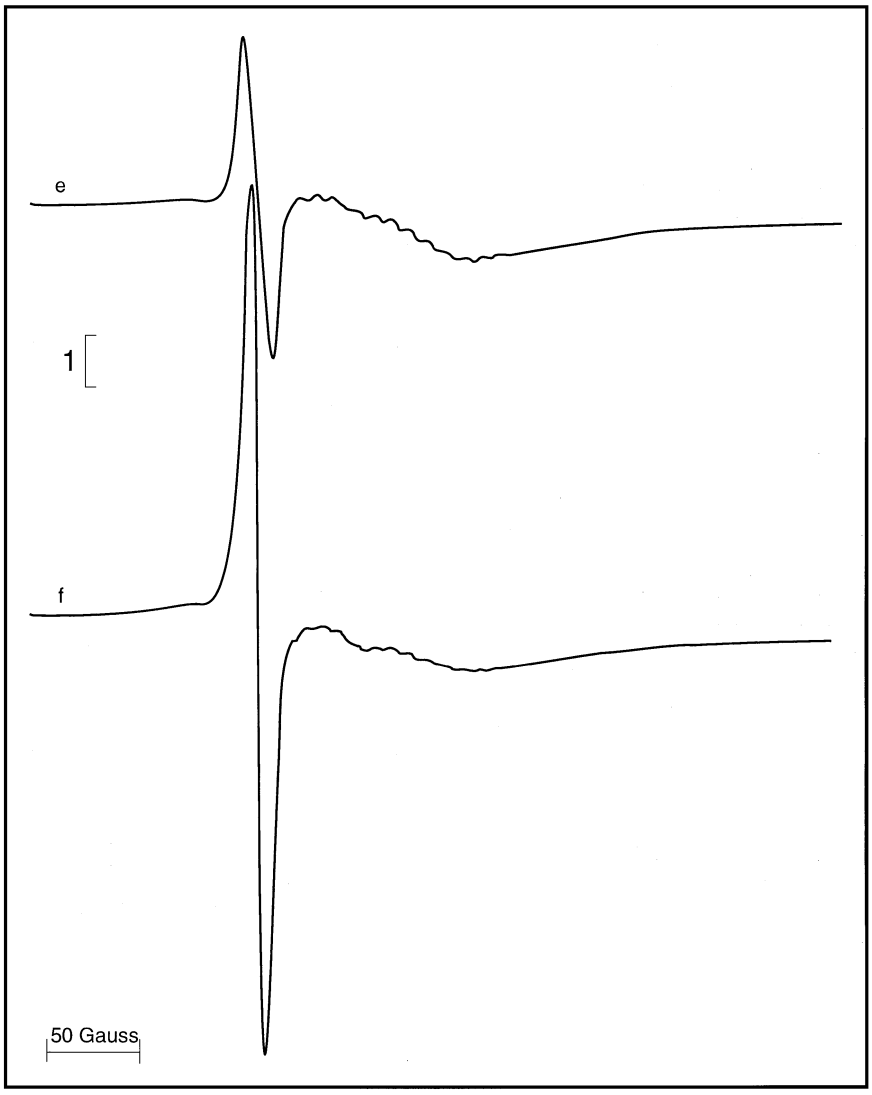

FIG. 2—*Continued*

illustrated in Fig. 6. Figure 6a shows the EPR spectrum of the 6Mo/HZSM-5 catalyst after stepwise heating from 273 to 973 K in a He stream and flashing with a He flow at 973 K for 0.5 h. During the pretreatment, a reduction induced by thermal treatment occurred apparently, and the signal C, which contains signals B, D, and E, was observed. In addition to the signals corresponding to the Mo^{5+} species, a new signal with an orthorhombic g tensor appeared. It has the g values as follows: $g_1 = 2.018$, $g_2 = 2.012$, and $g_3 = 2.005$. After the introduction of CH_4 into the reaction system for 30 min, the intensity of the signal decreased obviously, and the remaining parts (i.e., the g_1 and g_2 components) were obscured by a signal at about $g = 2.005$, which was the signal that resulted from the formation of carbonaceous deposits. The latter signal also superimposed with the low field part of the broad signal C to form a peak with the tip at $g = 2.005$. The intensity of the high field part of signal C decreased remarkably, similar to those shown in Figs. 3c and 3d. After the reaction with CH_4 for 1 and 3 h, this trend became more obvious, but we still could observe the signals D and E. The intensity of the signal corresponding to carbonaceous deposits increased sharply with the increasing of the reaction time on stream. The changes in the signal intensities of the overall Mo^{5+} and carbonaceous deposit with the time on stream are shown in Fig. 7. The signal intensity corresponding to carbonaceous deposits increased linearly, while that corresponding to the overall Mo^{5+} decreased sharply at first in the first half hour and then decreased smoothly with longer time on stream. It is interesting to note that even after 3 h of reduction and reaction by CH_4 at 973 K, we still could record the EPR signal that corresponds to the Mo^{5+} species.

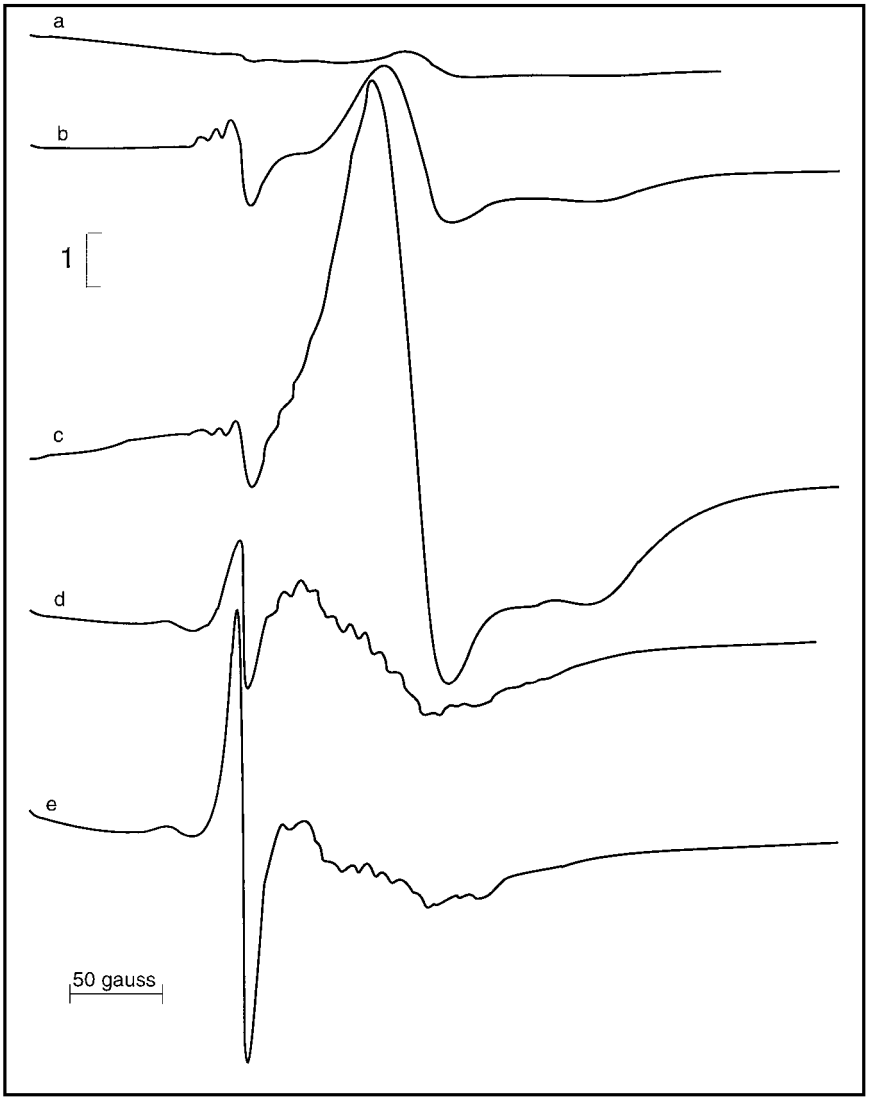

FIG. 3. ESR spectra of 6%Mo/HZSM-5 reduced at (a) 373 K for 1 h, (b) 573 K for 1 h, (c) 773 K for 1 h, (d) 973 K for 0.5 h, and (e) 973 K for 1 h.

3. Catalytic Evaluation of Mo/HZSM-5 Catalysts

Methane dehydro-aromatization under standard reaction conditions over the Mo/HZSM-5 catalysts is listed in Table 1. The amounts of C_8 and C_9 compounds are too small to be taken into account. Figure 8 shows the effect of Mo loading on r_{CH_4}, r_{AR}, and r_C after running the methane dehydro-aromatization reaction on Mo/HZSM-5 catalysts for 90 min. The depletion rate of methane, r_{CH_4}, increased significantly with increasing Mo loading in the range of 0–2% and then increased slightly with increasing Mo loading in the range of 2–10%. On the other hand, r_{CH_4} decreased with time on stream, as can be seen from Table 1. The effect of Mo loading on r_{AR} is obvious. Without the introduction of the Mo species, almost no aromatics could be formed. With an increase of Mo loading in the range of 0–2%, r_{AR} increased sharply to about 1100 nmol/(g cat s) after reaction for 90 min. With the Mo loading being increased further, r_{AR} reached a value of 1200 nmol/(g cat s) over the 6Mo/HZSM-5 catalyst and then r_{AR} decreased with the Mo loading from 6 to 10%. The change of the formation rate of carbonaceous deposits, r_C, with Mo loading is most interesting. It increased linearly with Mo loading from 0 to 2% and is almost constant in the Mo loading range of 2–10%. The results suggested that the conversion of methane was accompanied by the formation of carbonaceous deposits. In addition to the acid sites of HZSM-5, Mo species are also responsible for the formation of the carbonaceous deposits.

The changes of r_{CH_4}, r_{AR}, and r_C on the 6Mo/HZSM-5 catalyst together with the changes in the intensities of the overall Mo^{5+} and the carbonaceous deposit signals with the time on stream are presented in Fig. 7. In the first half hour, with the sharp decrease in the intensity of the overall Mo^{+5} signal, r_{AR} increases remarkably. Then, with further

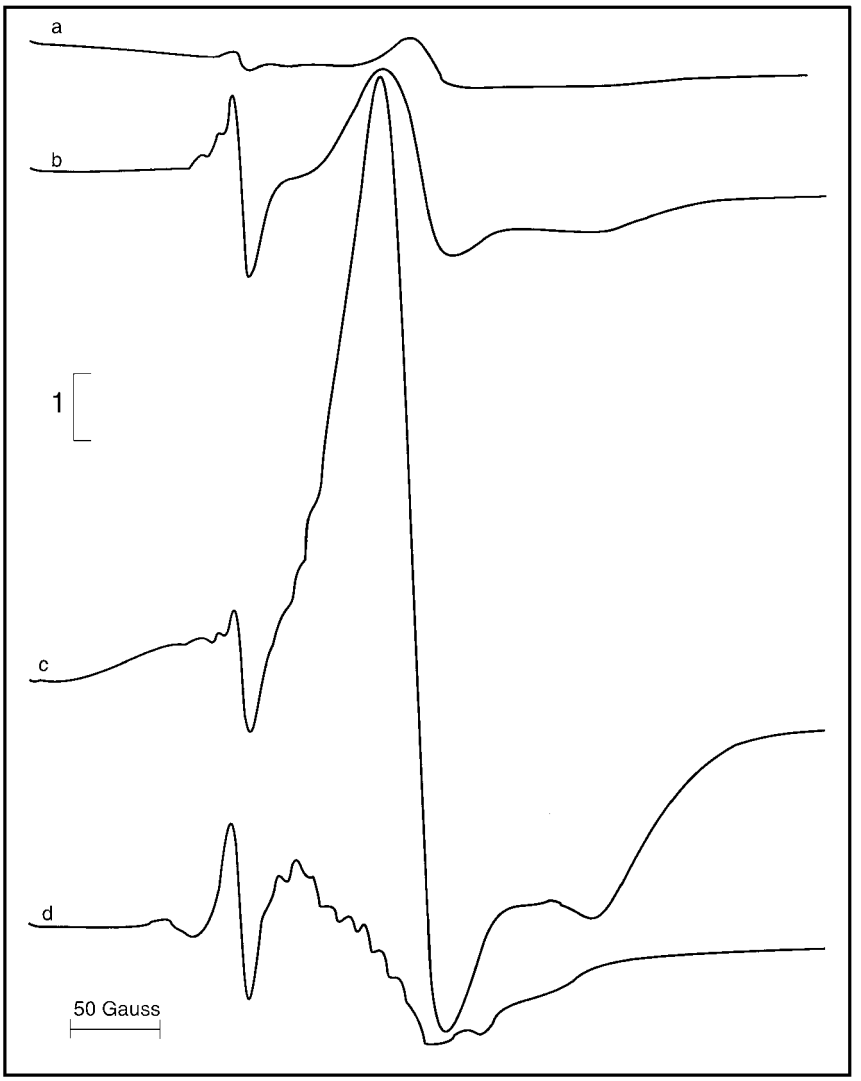

FIG. 4. ESR spectra of 10%Mo/HZSM-5 reduced at (a) 373 K for 1 h, (b) 573 K for 1 h, (c) 773 K for 1 h, and (d) 973 K for 0.5 h.

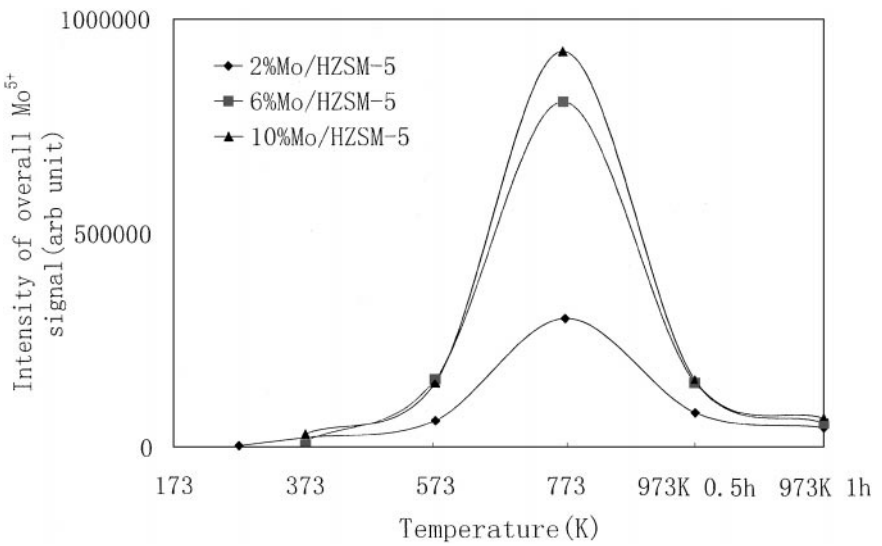

FIG. 5. The intensity of EPR signals of all Mo^{5+} species at different reduction temperatures.

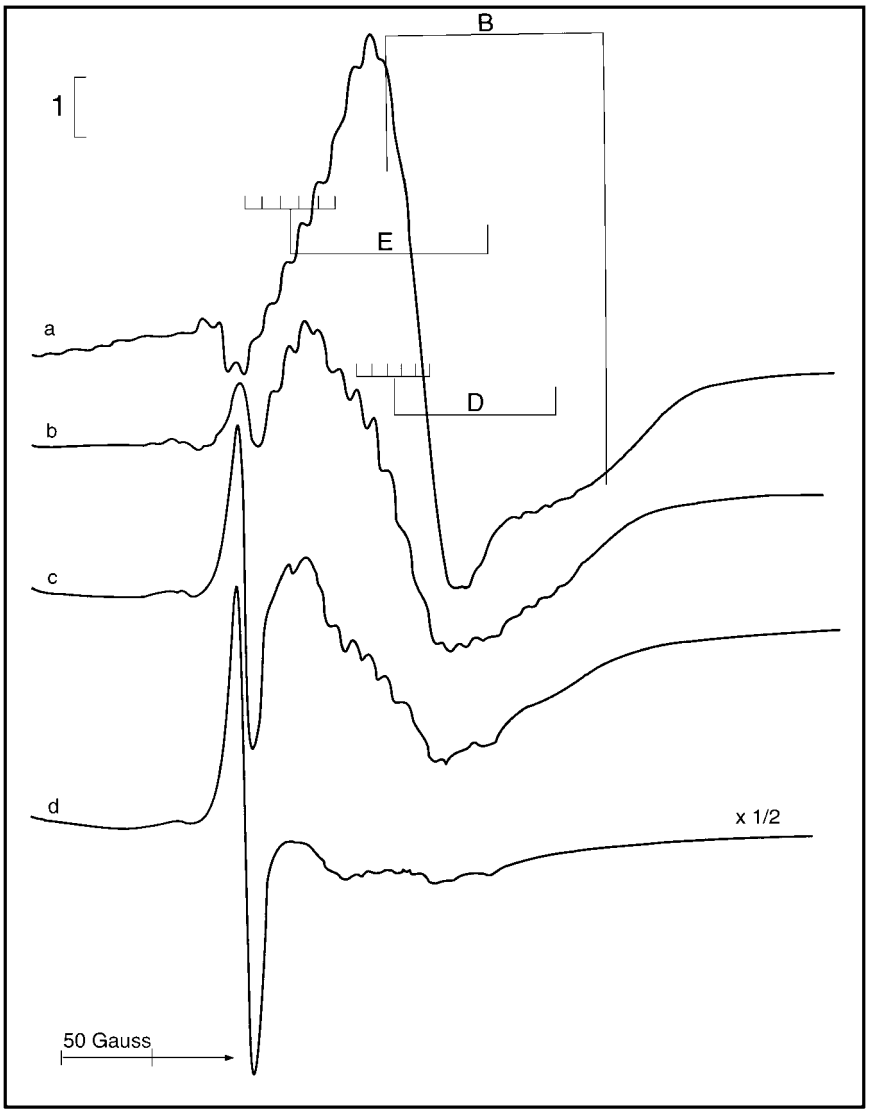

FIG. 6. ESR spectra on a 6%Mo/HZSM-5 sample recorded at the following times: (a) swept by He (15 ml/min) at 973 K for 0.5 h; (b) after (a) 0.5 h after CH_4 introduction; (c) after (b) 1 h after CH_4 introduction; (d) after (c), 3 h after CH_4 introduction.

decreases in the intensity of the overall Mo^{+5} signal, r_{AR} decreases a little. r_C also increases in the first half hour and then almost keeps constant, while the intensity of the carbonaceous deposit signal increases linearly, which is in agreement with the change of r_C.

DISCUSSION

1. *Assignment of EPR Signals Recorded on Mo/HZSM-5 Samples*

Figures 2–4 show that different Mo species on the Mo/HZSM-5 can be identified by the EPR technique after its stepwise reduction in a CH_4 atmosphere at different temperatures. The two smooth axial symmetric signals, A and B, appeared after the Mo/HZSM-5 was treated by CH_4 at room temperature, or at 373 and 573 K. Agudo *et al.* (5) suggested that most of the Mo species cannot migrate into the channels for the Mo/HZSM-5 prepared by impregnation because of its quite large volume of $Mo_7O_{24}^-$ and MoO_4^{2-} ions. Therefore, they may reside on the external surface in the form of molybdena crystallites. The shape and *g* values of the signals A and B are very similar to the EPR signal of the Mo^{5+} species, as if they are reduced and produced from the molybdena resided at the external surface of the SAPO-5 prepared by thermal dispersion of MoO_3 on SAPO-5 (4). The signal is also similar to the $Mo^{5+}{}_{6c}$ signal recorded on a Mo/SiO_2 catalyst prepared by impregnation and reduced by H_2 at 623 K (29).

It is noted that the signals A and B have an identical parallel feature but different perpendicular features. According to Refs. (4) and (29), signal A, which has a less anisotropic *g*

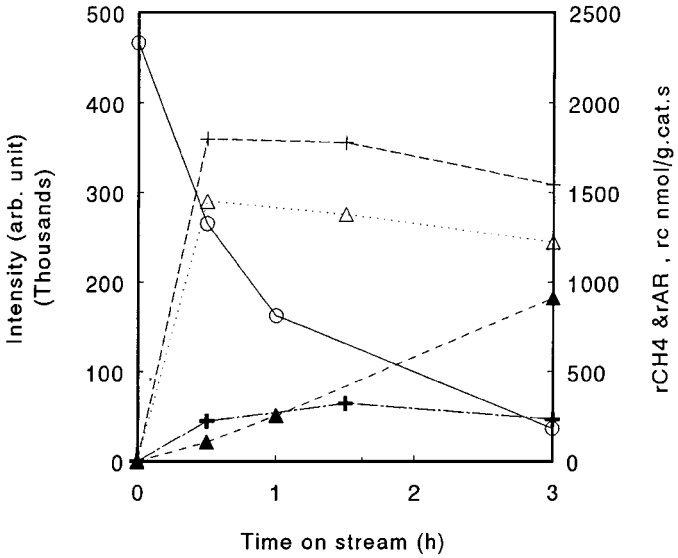

FIG. 7. The changes of the intensities of EPR signals related to the overall Mo^{5+} species (○) and coke (▲) and the r_{CH_4} (+), r_{AR} (△), and r_C (✚) with reaction time on 6Mo/HZSM-5.

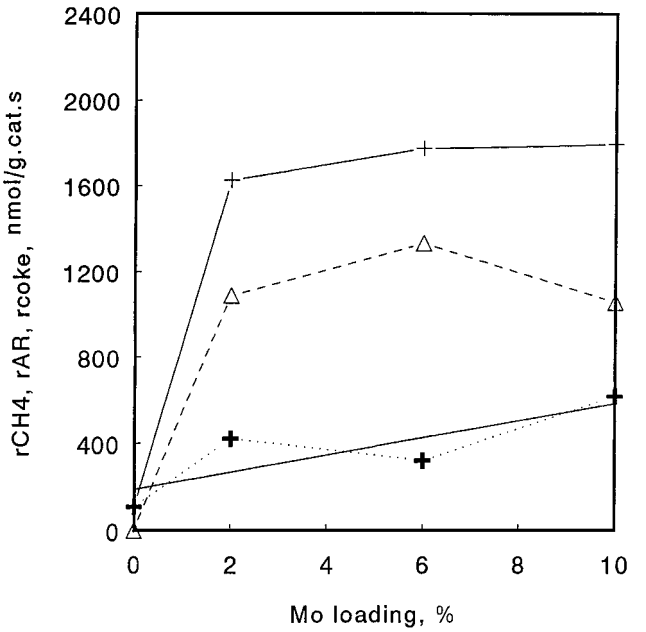

FIG. 8. The effect of Mo loading on r_{CH_4} (+), r_{AR} (△), r_C (✚) of methane aromatization on Mo/HZSM-5 catalysts (data were taken after the experiment was running for 90 min).

value, can be ascribed to the Mo species with a pressed octahedral coordination symmetry. Meanwhile, signal B shows the same value of $g_{\|}$ but a more anisotropic $g_{\perp}$. It implies that the Mo species corresponding to signal B has a similar coordination environment on the *x–y* plane, but with a different situation along the *z*-axis direction (33). A reasonable assignment of the signal B could be square-pyramidal coordination formed from the loss of one ligand in the Mo species corresponding to the signal A. Both of the species are located at the external surface of the HZSM-5 zeolite. In addition, the signal B is the biggest one among the signals of different Mo^{5+} species recorded. This indicates that a large part of Mo species residing on the external surface of HZSM-5 is in the form of square-pyramidal-coordinated MoO_x crystallites.

TABLE 1

Catalytic Performance of Methane over Mo/HZSM-5 Catalysts with Different Mo Loadings

Catalysts	Surface area (m^2/g)	Reaction time (min)	Reaction rate of CH_4 (nmol g^{-1} s^{-1})	Formation rate (nmol g^{-1} s^{-1}) of					
				CO	C_2	C_6H_6	C_7H_8	$C_{10}H_8$	Coke
HZSM-5	305	30	126.2						126.2
		90	109.3						109.3
		180	98.2						98.2
		360	25.5						25.5
2%Mo/HZSM-5	309	30	1648.0	57.7	48.6	785.5	29.7	475.1	251.5
		90	1626.3	12.5	66.7	731.9	34.8	357.9	422.1
		180	1316.1	7.4	78.3	663.7	35.8	265.4	341.6
		360	1229.1	4.7	94.5	548.6	32.9	174.9	373.5
6%Mo/HZSM-5	257	30	1798.6	75.3	46.2	942.0	30.7	479.3	224.0
		90	1776.2	17.4	58.4	983.4	42.6	351.5	322.7
		180	1542.0	8.8	72.2	940.6	43.3	239.9	233.9
		360	1284.6	4.8	90.0	832.0	42.0	149.5	165.8
10%Mo/HZSM-5	237	30	1899.2	100.1	45.6	788.7	21.5	296.6	644.5
		90	1798.5	12.6	66.3	821.3	36.9	238.1	621.9
		180	1520.4	7.0	83.1	749.7	40.1	140.0	492.0
		360	13427	0.0	98.5	651.1	38.0	88.03	166.3

Note. Reaction temperature, 973 K; atmospheric pressure; hourly space velocity of methane, 1500 h^{-1} g^{-1}.

With the increasing reduction temperature, signals D and E appeared. These two signals should be related to the Mo species not easily reduced by CH_4 (see Fig. 2d). The signals D and E overlapped with the previously appeared signals A and B and produced a broad and complicated signal. Both signals D and E had a set of six lines splitting. The corresponding hyperfine coupling constant is about 8 G. Such a kind of splitting lines has not been reported in the literature of EPR study of the Mo/HZSM-5 catalysts (30, 34).

Some oxide- or zeolite-supported Mo catalysts show hyperfine lines, which is due to the hyperfine interaction between the unpaired electron of Mo^{5+} and the odd isotopes of Mo, for example, ^{95}Mo and ^{97}Mo with natural abundance of 15.7% and 9.47%, respectively. The peak positions of these lines are usually at the low field region with a g value larger than g_e (2.0023). They are similar to those observed on Mo/SiO_2 samples (29). Usually, the hyperfine coupling constants caused by such an interaction is larger than 15 G, typically in the range of about 20–50 G in most cases. Such a kind of hyperfine structure can also be observed in our Mo/HZSM-5 catalysts, as shown in Figs. 2d and 2e, etc. On the other hand, for signals A and B, although they are coexisting, no such splitted signals could be observed. Therefore, the splitted signal observed in the signals D and E cannot be attributed to the interaction between the unpaired electron of Mo^{5+} and the odd isotopes of Mo. Moreover, if the 2Mo/HZSM-5 sample was first processed by stepwise reduction and then flushed with a He flow (15 ml/min) for 1 h, there is no difference between the recorded EPR spectrum and that shown in Fig. 2e. Therefore, we excluded the possibility that the splitted signals D and E resulted from the adsorption of the reduction gas or the products on the 2Mo/HZSM-5 surface. As a matter of fact, the splitting of the signals D and E resulted from the existence of the nearby odd nucleus moment. This is the case when the Mo species are located at positions closely associated with the ^{27}Al atom, which has odd nucleus moments ($I = 5/2$). Moreover, in HZSM-5-supported TMI catalysts, normally there are different cationic positions for the location of the TMI in zeolite cavities (30, 35). Therefore, we proposed that these two six-lines splitting signals D and E are corresponding to the mononuclear Mo cation located at two different positions in the lattice channel, denoted as $Al(I)\cdots MoO_x$ and $Al(II)\cdots MoO_x$. These are very similar to those reported in the cases of Cr/HZSM-5 and Cu/HZSM-5 (30, 35). Unfortunately, at the moment we cannot picture these two Mo species more clearly.

Summers *et al.* and Muicahy *et al.* (36) pointed out that the interaction between $Mo_7O_{24}^{6-}$ and the surface of Al_2O_3 may be the result of a two-step mechanism in acidic aqueous solutions. First, the adsorption of $Mo_7O_{24}^{6-}$ on the alumina surface by electrostatic force will lead to $Mo_7O_{24}^{6-}$ species loosely bonded to the alumina surface:

$$\equiv Al\text{–}OH_2^+ + Mo_7O_{24}^{6-} \Leftrightarrow \equiv Al\text{–}OH_2^+ \cdots Mo_7O_{24}^{6-}.$$

Second, the loosely bonded Mo species will condense with surface hydroxyls to form a tightly bonded species:

$$\equiv Al\text{–}OH_2^+ \cdots Mo_7O_{24}^{6-} \Leftrightarrow \equiv Al\text{–}O\text{–}Mo_7O_{23}^{5-} + H_2O.$$

A similar phenomenon has been reported in Mo/SiO_2 catalysts prepared by grafting and impregnation methods (27, 37).

In our Mo/HZSM-5 samples, a similar process may happen. Part of the Mo species will reside on the external surface, while part of them will migrate and diffuse into the channels of the HZSM-5 during calcination and preferentially locate at the position close to the framework Al. This is supported by the FT-IR results in which the intensity of the band at 3611 cm^{-1} decreased after introducing the Mo species on/in to the HZSM-5 catalyst (15, 38). On the other hand, the super-hyperfine interaction between the Mo^{5+} species and the ^{27}Al atoms ($I = 5/2$, natural abundance of 100%) will cause the EPR signals (D and E) to split into six lines. The relatively small coupling constant ($A \approx 8$ G) seems to support this assignment.

On the 2Mo/HZSM-5 sample, the signals D and E appeared after it was reduced by CH_4 at 573 K. The intensity of the high field part of the signal C, i.e., the signal D, is stronger than that of the low field part, i.e., the signal E. It is interesting to note that the intensity of signal D becomes much weaker compared with that of signal E after reduction at 973 K for 0.5 h. It implies that the Mo species related to the signal D are more easily reduced than the Mo species related to the signal E. The other possibility is the superimposition of signal B with signal D. The former signal corresponds to the much more easily reducible Mo species, which makes signal D, which appeared at 773 K, to decrease remarkably when the sample was reduced at 973 K. The fact that the smoothing and enlarging (773 K) of the high field part of signal C with increasing Mo loading seems to suggest that the latter possibility may be significant.

On the basis of the above discussion, we proposed that there are two kinds of Mo species on the Mo/HZSM-5 sample, which are located at different positions on/in the HZSM-5 zeolite. The first kind of Mo species is located at the outer surface. This kind of Mo species (corresponding to signals A and B) is easily reduced and shows no splitting spectra in their corresponding EPR spectra. We suggest that they are MoO_3oct crystallites (corresponding to signal A) which have pressed octahedral coordination and MoO_xsqu species (corresponding to signal B) with a square-pyramidal coordination (both may be in polynuclear form) located on the external surface. The second kind of Mo species is associated with the Al atom and located on/in the zeolite. There are two EPR signals, i.e., signal D and signal E; both of the signals show hyperfine structure with six splitting lines. Based on the reducibility of the corresponding Mo species, they can be denoted as the $Al(I)\cdots MoO_x$ and the $Al(II)\cdots MoO_x$ species, respectively. The Mo species

originally located on the external surface can migrate and diffuse into the channels of the HZSM-5 zeolite during calcination under the presence of acid sites that may serve as a powerful "trap" for the migrating ions (30) and locate onto the different positions close to the Al^{3+} ions. The reducibility of these two species is in the following order:

Mo species on the external surface
> Mo species in the channels.

More concretely speaking,

$$MoO_3oct \approx MoO_xsqu > Al(I)\cdots MoO_x > Al(II)\cdots MoO_x$$

These different Mo species are in turn associated with the EPR signals A, B, D, and E, respectively. On the other hand, the other Mo species could be covered by the MoO_3 crystallites (27). The proportion of all the four above-mentioned Mo species would strongly depend on the Mo loading and the preparation process of the catalysts.

2. Possible Precursors of the Active Sites for the Reaction

Solymosi *et al*. and Lunsford *et al*. have found that there is an induction period in methane dehydro-aromatization over the Mo/HZSM-5 catalyst (15, 22). During the early stage of the induction period, the complete oxidation of methane was dominant, leading to the formation of CO_2, CO, and H_2O. Lunsford *et al*. characterized the Mo/HZSM-5 catalyst by XPS and found that, during the initial induction period, CH_4 reduced the original Mo^{6+} ions to Mo_2C, accompanied by the formation of carbonaceous deposits (15, 39, 40). Finally, almost all Mo cations turned into Mo_2C, which is responsible for the initial activation of methane (9, 15). Possibly, the Mo_2C species are highly dispersed on the outer surface. Later, they found that preformation of Mo_2C on the HZSM-5 support, without coke deposition, could not completely eliminate the induction period. So Lunsford *et al*. supposed that the clean surface of Mo_2C might be too reactive in the forming of higher hydrocarbons and that a coke-modified Mo_2C surface might be the active species in the formation of ethylene (15). By using the XPS technique, Solymosi *et al*. found that Mo_2C was formed on the used catalyst and they regarded this as the active sites (22). They further examined the catalytic performance of the unsupported as well as the supported Mo_2C (9). It was concluded that besides Mo_2C the presence of some other Mo compounds, perhaps oxygen-deficient MoO_2, was also necessary for the activation of methane and for the promotion of the formation of ethylene from CH_x fragments. Later, Iglesia *et al*. (41) pointed out that Mo/HZSM-5 (4%Mo) forms CO_2, CO, H_2O, and carbon during initial contact with CH_4 at 950 K, as the Mo^{+6} cations are converted to oxycarbide species (MoO_xC_y) which activate CH_4. The results are consistent with isolated $(Mo_2O_5)^{2+}$ dimers interacting with two cation exchange sites which convert to MoO_xC_y during CH_4 reactions.

The EPR spectra of the 6Mo/HZSM-5, recorded after similar pretreatment used in the methane dehydroaromatization, revealed that a reduction induced by thermal treatment occurred, accompanying the appearance of a new signal with an orthorhombic g tensor. The g tensor has the characteristics of $g_1 = 2.018$, $g_2 = 2.012$, and $g_3 = 2.005$. These are very similar to the g value in Refs. (34) and (37) and can be attributed to O_2^- species. Osade *et al*. (42) reported that, in the oxidative coupling of methane, O_2^- may be the active species responsible for the initial activation of CH_4. The activation leads to the cleavage of one of the C–H bonds in methane. In the present case, since all the reactions were performed under nonoxidative conditions and O_2^- disappeared after the induction periods (about 30 min), O_2^- cannot be taken as the active species for the activation of methane. Probably, O_2^- formed from adsorbed O_2 and the lattice O^{2-} of MoO_3 is responsible for the formation of CO_2, CO, and H_2O in the early stage of the induction period of the reaction (22, 24).

On the other hand, despite the fact that the 6Mo/HZSM-5 catalyst was pretreated in the same way either in the EPR measurement or in its catalytic evaluation, the highest r_{CH_4} and r_{AR} were reached on the 6Mo/HZSM-5 catalyst in the first half hour on stream. Meanwhile, the intensity of the EPR signal for the overall Mo^{5+} species decreased obviously, but we can still detect quite a large amount of Mo^{5+} species. This is evident that much of the Mo species is still in their 5+ valence and part of the Mo^{5+} was further reduced into Mo_2C. The sharp decrease in the intensity of the EPR signal that corresponded to the overall Mo^{5+} in the first half hour is mainly due to the decrease in the intensity of signal B. The remarkable decrease in signal B corresponds to a further reduction of the Mo^{5+} species formed from the reduction of the MoO_3oct crystallites and the MoO_xsqu species residing on the external surface. We propose that the fully reduced Mo_2C species resulted from the MoO_3oct crystallites and the MoO_xsqu species are highly dispersed on the external surface, and the partially reduced Mo species formed from the Mo species associated with the Al atom are located in the channels of the zeolite.

CONCLUSIONS

EPR measurements show that there are two kinds of Mo species on/in the HZSM-5 zeolites: one resides on the external surface either in the form of MoO_3 crystallite with a pressed octahedral coordination or in the form of a MoO_x phase with a square-pyramidal coordination and the other is located inside the zeolites channels and may be in the form of $Al(I)\cdots MoO_x$ or $Al(II)\cdots MoO_x$, based on their reducibilities by CH_4. The reducibility of these four species are in the following sequence: $MoO_3oct \approx MoO_xsqu >$

$Al(I)\cdots MoO_x > Al(II)\cdots MoO_x$. The signal of O_2^- on the surface of the catalyst has been observed in the induction period of the catalytic reaction. During the induction period, the reduction of the MoO_3oct crystallites and the MoO_xsqu species reside at the external surface and are dominant, while at the same time the MoO_x species in the channels are partially reduced. After the induction period, fully reduced Mo species, Mo_2C, on the external surface and partially reduced Mo species, MoO_x, in the channels coexist in the catalyst. Combining the EPR study with the catalytic evaluation on the Mo/HZSM-5 catalysts, it seems to support the suggestion that possibly the fully reduced Mo_2C species together with the partially reduced MoO_x species are responsible for the reaction of methane dehydro-aromatization.

ACKNOWLEDGMENTS

Financial support of the Ministry of Science and Technology of China is gratefully acknowledged. The authors appreciate the reviewers' insightful comments and helpful suggestions.

REFERENCES

1. Abdo, S., and Howe, R. F., *J. Phys. Chem.* **87**, 1713 (1983).
2. Johns, J. R., and Howe, R. F., *Zeolites* **5**, 251 (1985).
3. Fierro, J. L. G., Conesa, J. C., and Agudo, A. L., *J. Catal.* **108**, 334 (1987).
4. Huang, M., Yao, J., Xu, S., and Meng, Ch., *Zeolites* **12**, 810 (1992).
5. Agudo, A. L., Benitez, A., Flerro, J. L. G., Palados, J. M., Nelra, J., and Cid, R., *J. Chem. Soc. Faraday. Trans.* **88**, 385 (1992).
6. Lee, C. W., Saint-Pierre, T., Azuma, N., and Kevan, L., *J. Phys. Chem.* **97**, 1811 (1993).
7. Wang, L., Tan, L., Xie, M., Xu, G., Huang, J., and Xu, Y., *Catal. Lett.* **21**, 35 (1993).
8. Shu, Y., Xu, Y., Wong, S.-T., Wang, L., and Guo, X., *J. Catal.* **170**, 11 (1997).
9. Solymosi, F., Cserenyi, J., Szoke, A., Bansagi, T., and Oszko, A., *J. Catal.* **165**, 150 (1997).
10. Weckhuygen, B. M., Wang, D., Rosynek, M. P., and Lunsford, J. H., *J. Catal.* **175**, 338 (1998). Weckhuygen, B. M., Wang, D., Rosynek, M. P., and Lunsford, J. H., *J. Catal.* **175**, 347 (1998).
11. Wong, S-T., Xu, Y., Wang, L., Liu, S., Li, G., Xie, M., and Guo, X., *Catal. Lett.* **38**, 39 (1996).
12. Wang, L., Xu, Y., Wong, S.-T., Cui, W., and Guo, X., *Appl. Catal. A: Gen.* **152**, 173 (1997).
13. Chen, L., Lin, L., Xu, Z., Zhang, T., and Li, X., *Catal. Lett.* **39**, 169 (1996).
14. Liu, S., Don, Q., Ohnishi, R., and lchikawa, M., *J. Chem. Soc., Chem. Commum.* **15**, 1455 (1997).
15. Wang, D., Rosynek, M. P., and Lunsford, J. H., *J. Catal.* **169**, 347 (1997).
16. Chen, L., Lin, L., Xu, Z., Lian, X., Zhang, T., and Li, X., *J. Catal.* **157**, 190 (1995).
17. Xu, Y., Liu, S., Wang, L., Xie, M., and Guo, X., *Catal. Lett.* **30**, 135 (1995).
18. Xu, Y., Shu, Y., Liu, S., Huang, J., and Guo, X., *Catal. Lett.* **35**, 233 (1995).
19. Xu, Y., Liu, W., Wong, S.-T., Wang, L., and Guo, X., *Catal. Lett.* **40**, 207 (1996).
20. Solymosi, F., Szoke, A., and Cserenyi, J., *Catal. Lett.* **39**, 157 (1996).
21. Schuurman, Y., Decamp, T., Pantazidis, A., Xu, Y. D., and Mirodatos, C., *Stud. Surf. Sci. Catal.* **109**, 351 (1997).
22. Solymosi, F., Erdoholyi, A., and Szoke, A., *Catal. Lett.* **32**, 43 (1995).
23. Liu, W., Xu, Y., Wong, S.-T., Wang, L., Qiu, J., and Yang, N., *J. Mol. Catal. A: Chem.* **120**, 257 (1997).
24. Jiang, H., Wang, L., Cui, W., and Xu, Y., *Catal. Lett.* **57**, 95 (1999).
25. Khulbe, K. C., Manu, R. S., and Ternan, M., *Can. J. Chem.* **566**, 1769 (1978).
26. Meriaudeau, P., Che, M., and Tench, A. J., *Chem. Phys. Lett.* **31**, 547 (1975).
27. Louis, C., Che, M., and Anpo, M., *J. Catal.* **141**, 453 (1993).
28. Che, M., Dyrel, K., and Louis, C., *J. Phys. Chem.* **89**, 4526 (1985).
29. Louis, C., and Che, M., *J. Phys. Chem.* **91**, 2875 (1987).
30. Kucherov, A. V., and Slinkin, A. A., *Zeolites* **7**, 38 (1987).
31. Kucherov, A. V., and Slinkin, A. A., *Zeolites* **7**, 583 (1987).
32. Lange, J. P., Gutsze, A., and Karge, H. G., *J. Catal.* **114**, 136 (1988).
33. Che, M., Fournier, M., and Launay, J. P., *J. Phys. Chem.* **17**, 1954 (1987).
34. Huang, M.-M., John, J. R., and Howe, R. F., *J. Phys. Chem.* **92**, 1291 (1988).
35. Dedecek, J., Sobalik, Z., Tvaruzkova, Z., Kaucky, D., and Wichterlova, B., *J. Phys. Chem.* **99**, 16327 (1995). Wichterlova, B., Dedecek, J., and Vondrova, A., *J. Phys. Chem.* **99**, 1065 (1995).
36. Summer, J. C., and Ausen, S. A., *J. Catal.* **52**, 445 (1978). Muicahy, F. M., Fay, M. J., Proctor, A., Houalla, M., and Hercules, D. M., *J. Catal.* **124**, 231 (1990).
37. Latef, A., Aissi, C. F., and Guelton, M., *J. Catal.* **119**, 368 (1989).
38. Liu, W., and Xu, Y., *J. Catal.* **185**, 386 (1999).
39. Wang, D., Lunsford, J. H., and Rosynek, M. P., *Top. Catal.* **3**, 289 (1996).
40. Weckhuygen, B. M., Rosynek, M. P., and Lunsford, J. H., *Catal. Lett.* **52**, 31 (1998).
41. Borry, R. W., III, Lu, E. C., Kim, Y. H., and Iglesia, E., *Stud. Surf. Sci. Catal.* **119**, 403 (1998).
42. Osada, Y., Koike, S., Fudushima, T., and Ogasawara, S., *Appl. Catal.* **59**, 59 (1990).